

SARMAE: Masked Autoencoder for SAR Representation Learning

Danxu Liu^{1,4*}, Di Wang^{2,4*}, Hebaixu Wang^{3,4*}, Haoyang Chen^{2,4*}, Wentao Jiang²
Yilin Cheng^{4,5}, Haonan Guo^{4,6}, Wei Cui^{1†}, Jing Zhang^{2,4†}

¹School of Information and Electronics, Beijing Institute of Technology, Beijing, China

²School of Computer Science, Wuhan University, Wuhan, China

³School of Electronic Information, Wuhan University, Wuhan, China

⁴Zhongguancun Academy, Beijing, China

⁵School of Data Science, Fudan University, Shanghai, China

⁶State Key Laboratory of Information Engineering in Surveying, Mapping and Remote Sensing, Wuhan University, Wuhan, China

Abstract

Synthetic Aperture Radar (SAR) imagery plays a critical role in all-weather, day-and-night remote sensing applications. However, existing SAR-oriented deep learning is constrained by data scarcity, while the physically grounded speckle noise in SAR imagery further hampers fine-grained semantic representation learning. To address these challenges, we propose SARMAE, a Noise-Aware Masked Autoencoder for self-supervised SAR representation learning. Specifically, we construct SAR-IM, the first million-scale SAR dataset, with additional paired optical images, to enable large-scale pre-training. Building upon this, we design Speckle-Aware Representation Enhancement (SARE), which injects SAR-specific speckle noise into Masked Autoencoder to facilitate noise-aware and robust representation learning. Furthermore, we introduce Semantic Anchor Representation Constraint (SARC), which leverages paired optical priors to align SAR features and ensure semantic consistency. Extensive experiments across multiple SAR datasets demonstrate that SARMAE achieves state-of-the-art performance on classification, detection, and segmentation tasks. Code, data, and models available at [SARMAE](#).

1. Introduction

Synthetic Aperture Radar (SAR) imagery, characterized by its all-weather, day-and-night imaging capability, serves as a critical source of remote sensing information [2, 4, 20, 28, 60, 98]. Owing to this robustness against challenging atmospheric and illumination variations, SAR has been widely applied in various domains such as ocean

*Equal contributions.

†Corresponding authors.

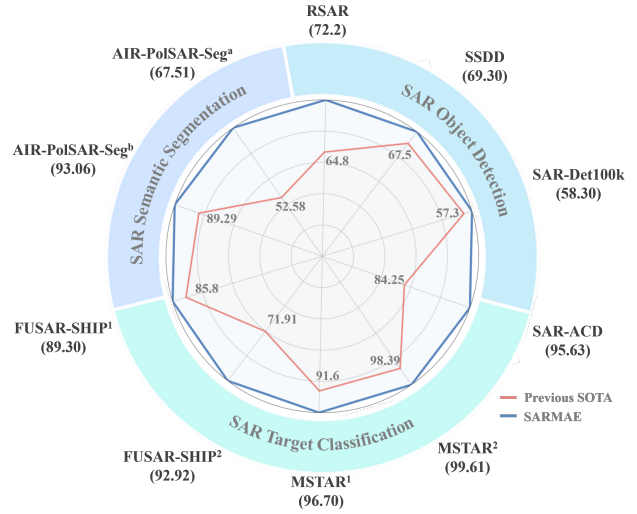


Figure 1. SARMAE outperforms SOTA methods on multiple datasets. ¹: 40-SHOT; ²: 30% labeled. ^a: Multi-classes; ^b: Water.

monitoring, disaster assessment, and urban scene analysis [46, 48, 49, 51, 59, 80, 83].

The emergence of deep learning has greatly advanced SAR image interpretation [96]. Early approaches were typically designed for specific tasks [31], exhibiting limited generalization across diverse downstream applications. To overcome this limitation, subsequent representation learning methods adopted the pretraining–finetuning paradigm [15, 33, 34, 43, 81] to achieve unified and generalized interpretation. In this context, self-supervised pre-training methods [1, 7, 25] have shown great potential for learning transferable representations from unlabeled data, thereby inspiring the development of analogous frameworks tailored for SAR imagery [16, 35].

Despite these advances, existing SAR representation learning methods still face several limitations. First, due to the high cost of SAR data acquisition, current studies often lack sufficiently large and diverse pretraining datasets, limiting the ability of models to learn general-purpose SAR representations [11, 29, 57, 62–64]. Second, the unique imaging mechanism of SAR introduces severe speckle noise, leading to low semantic content and weak structural cues [10, 28, 50, 68–70]. However, prevailing pre-training methods simply adopt strategies borrowed from optical imagery [15], overlooking the physical nature of SAR noise. Third, pretraining paradigms that rely exclusively on SAR data are inherently limited by its semantic scope [8, 37, 52]. This overlooks the valuable guidance that could be drawn from complementary, information-rich modalities such as optical imagery [19]. Consequently, the learned representations often lack the semantic richness and generalizability required for diverse downstream tasks.

To address these challenges, we propose SARMAE, a Masked Autoencoder (MAE) [25]-based framework for SAR representation learning. Specifically, we construct SAR-1M, the first million-scale SAR dataset that covers diverse scenes, targets, and sensor characteristics, providing over 1.3 million SAR images for large-scale pretraining. We then introduce Speckle-Aware Representation Enhancement (SARE), which explicitly incorporates SAR imaging noise during pretraining. By reconstructing the original image from perturbed inputs injected with SAR-specific speckle noise, SARE encourages the network to perceive and capture the intrinsic speckle characteristics of SAR imagery, thereby learning noise-resistant representations and improving robustness. Finally, we design Semantic Anchor Representation Constraint (SARC). Considering the more discernible semantic structure of optical imagery, SARC aligns SAR features with geographically paired optical priors to guide the encoder learning. This alignment enforces semantic consistency, accelerates model convergence, and enhances the generalization of pretrained representations. Extensive experiments on various downstream tasks demonstrate that SARMAE achieves state-of-the-art performance across multiple SAR datasets, as illustrated in Fig. 1. Our main contributions are summarized as follows:

- We propose SAR-1M, the first million-scale SAR dataset covering diverse resolutions, scenes, scales, targets, and task scenarios, along with additional paired optical images, enabling large-scale pretraining.
- We introduce Speckle-Aware Representation Enhancement to enforce robust feature learning by reconstructing inputs corrupted with physically grounded speckle noise, thereby mitigating the adverse impact of noise on SAR feature extraction.
- We design Semantic Anchor Representation Constraint to align SAR features with paired optical priors to regular-

ize encoder learning, ensuring semantic consistency and enhancing representation generalization.

2. Related work

2.1. SAR Datasets for Representation Learning

Many SAR datasets are characterized by extreme specialization, either focusing on single-category targets such as MSTAR [12] or SSDD [88], or being curated for a single downstream task, as exemplified by the detection dataset SAR-Det100k [38]. Beyond this narrow scope lies a more fundamental limitation: the lack of scale across the community’s available resources. Consequently, even state-of-the-art pretrained models such as SARATR-X [35] and SUMMIT [16] are trained on relatively small datasets containing only 180k and 560k images, respectively. This combination of limited semantic diversity, task specificity, and insufficient data volume imposes a clear ceiling on model performance and hinders the development of generalizable pretraining paradigms for SAR representation learning. To this end, we introduce SAR-1M, the first million-scale SAR dataset spanning diverse resolutions, imaging scales, object categories, and task scenarios, providing the scale and semantic richness required for large-scale pretraining.

2.2. SAR Representation Learning

Recently, large-scale self-supervised pretraining paradigms have been introduced to remote sensing [21, 66, 67, 71]. SeCo [47] adopts a MoCo-style [24] framework for scene classification, while RVSA [62] leverages MAE [25] pretraining to obtain initial weights and further introduces rotated varied-size window attention to enhance representation learning. SatMAE [9] extends MAE to multispectral and multitemporal imagery, and ScaleMAE [53] introduces scale-aware masking to improve generalization across spatial resolutions. Other approaches aim to learn task-agnostic representations by leveraging massive unlabeled datasets across diverse modalities [18, 26, 58, 65, 79]. However, these efforts remain predominantly focused on optical imagery, overlooking the unique characteristics of SAR data—particularly its inherent speckle noise and distinct imaging physics.

Motivated by the success of unsupervised pretraining paradigms in optical imagery, several studies have explored self-supervised SAR representation learning. BIDFC [85] adopts a contrastive learning framework with weak supervision, while SAR-JEPA [32] leverages masked autoencoding and local reconstruction to extract spatial features. MSFA [38] further introduces a multi-stage filter-based strategy. Although these approaches provide valuable insights, they remain constrained to single-task settings. To address these limitations, recent works have proposed unified pretraining frameworks tailored for SAR imagery.

Model	Pretrain Dataset	Modality	Task Types	Size	Targets	Resolution	Band
MSFA [38]	DOTA [76]	OPT	Det.	-	-	-	-
SAR-JEPA [32]	SAR-JEPA	SAR	Cls.	90k	21	0.3m-25m	C/X
SARATR-X [35]	SAR-VSA	SAR	Cls.&Det.	180k	25	0.1m-25m	C/X/Ku/Ka
SUMMIT [16]	MuSID	SAR	Cls.&Det.	560k	41	0.1m-25m	C/X
SARMAE	SAR-1M	SAR&OPT	Cls.&Det.&Seg.	1.3M SAR/2.3M Total*	57	0.1m-60m	C/X/Ku/Ka

Table 1. Pretraining datasets for SAR Representation Learning. *Our dataset comprises 1.3M SAR and 1M paired OPT images.

SARATR-X [35] employs a HiViT [89] with a two-stage self-supervised learning framework for unified SAR target detection and classification, while SUMMIT [16] adopts a masked image modeling framework with multiple auxiliary self-supervised tasks to adapt to diverse downstream scenarios. These two models demonstrate the feasibility of learning general-purpose SAR representations through large-scale pretraining. However, both methods overlook the intrinsic physical priors of SAR imaging and rely solely on low-quality, noise-contaminated data for pretraining, which limits the semantic richness of their learned representations. In this paper, we propose SARMAE, a noise-aware framework that explicitly models realistic speckle characteristics during pretraining and incorporates high-fidelity paired optical imagery as semantic guidance, thereby enhancing the model’s capability to learn robust and semantically consistent representations from complex SAR data.

3. Method

In this section, we first introduce the constructed SAR-1M dataset. Based on this foundation, we then present SAR-MAE, which incorporates two key innovations: Speckle-Aware Representation Enhancement (SARE) and Semantic Anchor Representation Constraint (SARC).

3.1. SAR-1M Dataset

Existing public datasets for SAR image analysis are hampered by limitations in scale and task diversity. To overcome these obstacles, we construct a million-scale, multi-source dataset, termed SAR-1M.

SAR-1M is a curated aggregation of 18 publicly available datasets, as illustrated in Fig. 2. During data collection, we adhered to two core principles: semantic richness and sensor diversity. For semantic richness, we selected datasets covering representative object categories such as ship, aircraft, vehicle, and bridge, as well as land-cover types including bareland, rangeland, agricultural land, and mountains. In addition, SAR-1M incorporates event-related scenes (e.g., earthquake), further enriching the contextual variety. Notably, many of these datasets were originally designed for detection or segmentation tasks, meaning that their samples typically have larger spatial coverage and richer fine-grained semantics. As a result, SAR-1M encom-

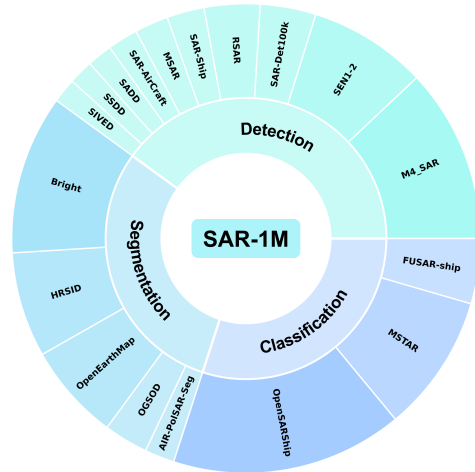


Figure 2. The organization of data sources in SAR-1M.

passes over 50 distinct categories, offering extensive semantic diversity and enhancing the representation capability of SAR-oriented models.

Beyond semantic diversity, SAR-1M integrates imagery from multiple sensors: Sentinel-1, Gaofen-3, RadarSat-2, Terma A/S, and TerraSAR-X, covering multiple frequency bands (C, X, Ku, Ka) and polarization modes (HH, HV, VV, VH). These diverse configurations yield data with varying ground resolutions and scattering characteristics, enriching the representation of different imaging conditions. Moreover, as several source datasets were collected on a global scale (e.g., SEN1-2 [55]), SAR-1M exhibits remarkable geographical diversity, which further enhances the generalization and adaptability of pretrained models.

Unlike existing SAR-only datasets, SAR-1M also incorporates geographically aligned SAR–optical pairs, resulting in approximately 2.3 million samples. Even when restricted to the SAR modality, it still comprises over 1.3 million images, providing ample scale for robust pretraining.

It is worth noting that the number of channels in the originally collected SAR images varies across datasets. To ensure consistency for unified pretraining, each polarization mode was expanded to a three-channel format when the original image contained a number of channels not equal to three. A detailed comparison between SAR-1M and existing SAR pretraining datasets is presented in Table 1.

3.2. SARMAE

3.2.1. Overall framework

Fig. 3 illustrates the overall framework of SARMAE for pretraining, which consists of a SAR branch and an optical branch. The SAR branch follows the architecture of MAE [25], where the encoder adopts a ViT backbone and the decoder is composed of multiple Transformer layers same as the original MAE. The optical branch employs a frozen DINOv3 [56] network that shares the same ViT-based encoder architecture as the SAR branch, facilitating subsequent feature alignment between the two modalities.

During pretraining, a SAR image is fed into the SAR branch, following the same procedure as MAE. To cope with the speckle noise inherent in SAR imagery, we explicitly introduce it into the SAR branch and enforce the network to learn effective denoising representations. This mechanism, termed Speckle-Aware Representation Enhancement (SARE), improves the model’s ability to capture robust and discriminative SAR features. Furthermore, considering that some SAR images are paired with optical counterparts, we propose a Semantic Anchor Representation Constraint (SARC) to fully exploit such multimodal correspondence. In this design, the optical image is passed through the frozen DINOv3 branch to obtain discriminative semantic features, which serve as semantic anchors to guide the SAR encoder’s representation learning. This constraint not only facilitates model convergence but also enhances generalization capability.

It is worth noting that if a SAR image does not have a paired optical counterpart, it is only processed by the SAR branch. The following sections provide detailed explanations of SARE and SARC.

3.2.2. Speckle Aware Representation Enhancement

Unlike additive Gaussian noise, speckle is a multiplicative phenomenon arising from the coherent summation of backscattered signals within a resolution cell. For a multi-look SAR intensity image, the observed intensity Z is the result of incoherently averaging L independent single-look measurements $\{I_i\}_{i=1}^L$, where each I_i follows an exponential distribution with mean \bar{I} equal to the true backscattering intensity. This process is formally described as:

$$Z = \frac{1}{L} \sum_{i=1}^L I_i, \quad \text{where } I_i \sim \text{Exp}(\bar{I}), \quad E[I_i] = \bar{I}. \quad (1)$$

Consequently, the multi-look intensity Z follows a Gamma distribution, with its probability density function (PDF) given by:

$$p_Z(z|\bar{I}, L) = \frac{L^L}{\Gamma(L)\bar{I}^L} z^{L-1} \exp\left(-\frac{Lz}{\bar{I}}\right), \quad z \geq 0, \quad (2)$$

where $\Gamma(\cdot)$ is the Gamma function, L is the number of looks, and the mean of Z is $E[Z] = \bar{I}$. Equation 2 provides

a physically grounded model for speckle, explicitly showing that the observed pixel intensity z is a random variable drawn from a distribution whose shape is determined by the true scene signal \bar{I} . This statistical entanglement is precisely what confuses standard pre-training paradigms and motivates our physics-informed design.

Grounded in this statistical model, we design SARE. Instead of merely reconstruct the original (and already noisy) masked patches, we reformulate the self-supervised task so that the model is trained to denoise a synthetically corrupted version of the input back to the original SAR patch. Specifically, for any given input SAR patch x , it is treated as the best available estimate of the true signal (*i.e.*, $x \approx \bar{I}$). A more heavily corrupted observation x' is then synthesized by sampling from the Gamma distribution with a reduced synthetic look number L_{syn} :

$$x'(i, j) \sim \text{Gamma}\left(L_{\text{syn}}, \frac{x(i, j)}{L_{\text{syn}}}\right). \quad (3)$$

This construction preserves the pixel-wise mean $E[x'(i, j)] = x(i, j)$ while increasing the variance through the lower look number. Here, L_{syn} is chosen to be significantly smaller than the effective number of looks in the original patch, ensuring that the synthesized patch x' exhibits a higher noise level.

The pre-training task is then formulated as a denoising reconstruction objective. Given the synthetically corrupted patch x' , we apply random masking with a high masking ratio (75% following MAE) to obtain a masked version \tilde{x}' , retaining only a subset of visible patches indexed by \mathcal{V} . The visible patches are fed to the encoder E_{SAR} to produce latent representations, which are then processed by the decoder D along with learnable mask tokens to reconstruct the original patch x . The reconstruction loss of SARE is defined as the mean squared error (MSE) between the predicted patches and the corresponding original patches in the masked regions \mathcal{M} :

$$\mathcal{L}_{\text{SARE}} = \frac{1}{|\mathcal{M}|} \sum_{p \in \mathcal{M}} \|D(E_{\text{SAR}}(\tilde{x}'))_p - x_p\|_2^2, \quad (4)$$

where p indexes the masked patch positions, $|\mathcal{M}|$ denotes the number of masked patches, $D(E_{\text{SAR}}(\tilde{x}'))_p$ represents the reconstructed patch at position p , and x_p is the corresponding ground-truth patch from the original input. This formulation trains the model to map noisy inputs to clean and complete representations. By doing so, the encoder learns features that are robust to the statistical fluctuations inherent to SAR imaging and are largely disentangled from speckle noise.

Notably, in our implementation, in addition to the Gamma model, we also incorporate Rayleigh, Gaussian, and Uniform noise, to generate more diverse corrupted samples and further improve model robustness.

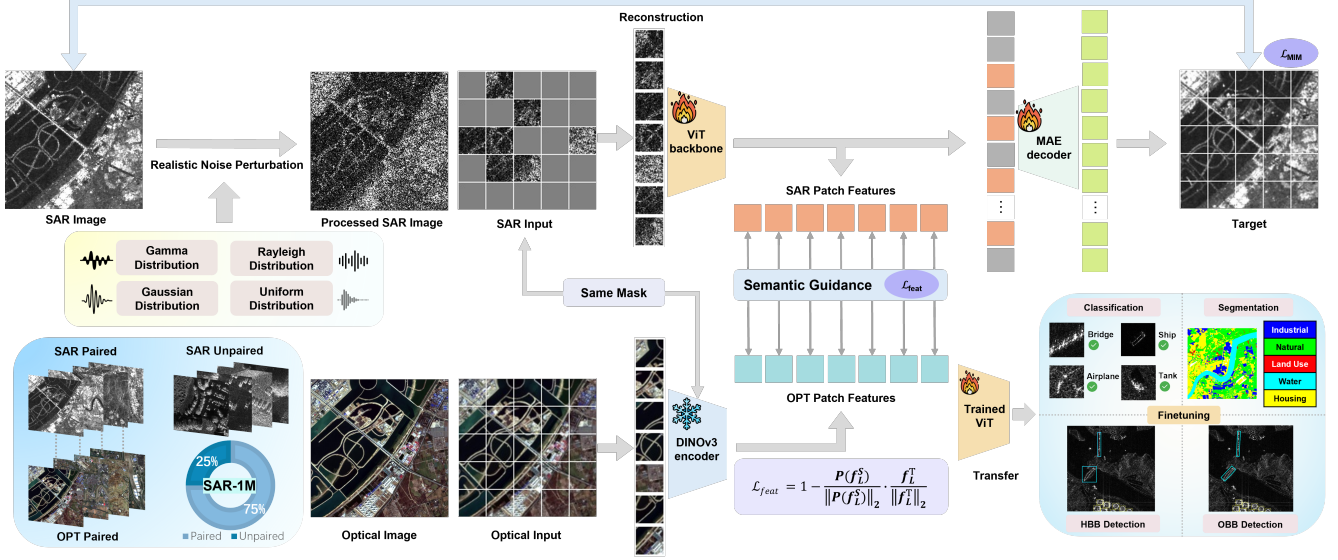


Figure 3. Overview of the SARMAE pretraining framework. The framework consists of two branches: (i) a SAR branch following the MAE architecture with Speckle-Aware Representation Enhancement (SARE) to handle inherent speckle noise, and (ii) an optical branch using a frozen DINOv3 encoder. For paired SAR-optical data, Semantic Anchor Representation Constraint (SARC) aligns SAR features with semantic-rich optical representations. Unpaired SAR images are processed solely through the SAR branch.

3.2.3. Semantic Anchor Representation Constraint

While SARE improves robustness to speckle noise, it does not provide the high-level semantic cues that are readily available in paired optical imagery. To this end, we introduce the SARC.

For a given co-registered image pair (I_{SAR}, I_{OPT}) , the SAR image is masked using the MAE strategy and passed through E_{SAR} to obtain embeddings for the visible patches,

$$f_{SAR} = \{f_{SAR}^i\}_{i \in \mathcal{V}}, \quad (5)$$

where \mathcal{V} denotes the set of visible patch indices. Concurrently, the unmasked optical image is processed by the frozen encoder E_{OPT} to produce a full sequence of anchor embeddings,

$$f_{OPT} = \{f_{OPT}^i\}_{i=1}^N. \quad (6)$$

Then, we enforce that the representation of a SAR patch should be semantically aligned with its spatially corresponding optical patch. This is achieved through a patch-wise cosine distance loss. For each visible SAR patch embedding f_{SAR}^i at spatial position $i \in \mathcal{V}$, the optical patch embedding f_{OPT}^i at the same location serves as the semantic target. Accordingly, the SARC loss is defined as the mean cosine distance over all visible patches:

$$\mathcal{L}_{SARC} = \frac{1}{|\mathcal{V}|} \sum_{i \in \mathcal{V}} \left(1 - \frac{f_{SAR}^i \cdot f_{OPT}^i}{\|f_{SAR}^i\|_2 \|f_{OPT}^i\|_2} \right). \quad (7)$$

This objective directly minimizes the cosine distance between the SAR and optical feature vectors, enforcing strong

directional alignment in the embedding space. As a result, the SAR encoder E_{SAR} learns not only SAR-specific structural cues, but also embeds them in a feature space shaped by the discernible semantic structure provided by the frozen optical teacher.

Overall Pre-training Objective. The overall pre-training loss consists of two components: the SARE loss and the SARC loss:

$$\mathcal{L}_{pretrain} = \mathcal{L}_{SARE} + \lambda \mathcal{L}_{SARC}, \quad (8)$$

where λ balances the modality-specific reconstruction objective and the cross-modal semantic alignment. In our implementation, we set $\lambda = 0.1$. Through this dual-objective optimization, the SAR encoder learns representations that are simultaneously robust to speckle noise and enriched with meaningful semantics, enabling superior performance across downstream perception tasks.

4. Experiments

In this section, we conduct comprehensive experiments to evaluate the proposed method across multiple downstream tasks, including SAR target classification, object detection, and semantic segmentation. We also assess the effectiveness of the SAR-1M dataset and the contributions of the proposed SARE and SARC modules through ablation studies. We initialize the SAR-branch encoder with ViT weights pretrained on ImageNet [11] using MAE [25]. The model is trained for 300 epochs using AdamW (learning rate =

Method	FUSAR-SHIP		MSTAR		SAR-ACD
	40-shot	30%	40-shot	30%	30%
ResNet-50 [23]	-	58.41	-	89.94	59.70
Swin Transformer [41]	-	60.79	-	82.97	67.50
Beit [1]	59.70	71.13	40.70	69.75	79.77
LoMaR [36]	82.70	-	77.00	-	-
SAR-JEPA [32]	85.80	-	91.60	-	-
SUMMIT [16]	-	71.91	-	98.39	84.25
Copernicus FM [73]	87.61	-	-	-	92.63
CROMA [18]	83.71	-	-	-	88.99
SARMAE(ViT-B)	89.30	92.92	96.70	99.61	95.06
SARMAE(ViT-L)	90.86	92.80	97.24	98.92	95.63

Table 2. Performance comparison (Top1 Accuracy, %) of different methods on the target classification task.

Method	SARDet-100k	SSDD	Method	RSAR
ImageNet [11]	52.30	66.40	RoI-Transformer [13]	35.02
Deformable DETR [97]	50.00	52.60	Def. DETR [97]	46.62
Swin Transformer [41]	53.80	40.70	RetinaNet [39]	57.67
ConvNeXt [42]	55.10	-	ARS-DETR [84]	61.14
CATNet [14]	-	64.66	R3Det [82]	63.94
MSFA [38]	56.40	-	ReDet [22]	64.71
SARATR-X [35]	57.30	67.50	O-RCNN [87]	64.82
SARMAE(ViT-B)	57.90	68.10	SARMAE(ViT-B)	66.80
SARMAE(ViT-L)	63.10	69.30	SARMAE(ViT-L)	72.20

Table 3. Performance comparison (mAP, %) of different methods on horizontal and oriented object detection tasks.

1×10^{-3} , weight decay = 0.05) with a batch size of 1024 and a cosine learning-rate schedule. All the experiments are performed on NVIDIA A800 GPU. All fine-tuning details are provided in the supplementary material.

4.1. Main Results

We compare SARMAE with existing state-of-the-art methods. In addition to general-purpose visual representation models such as ImageNet-pretrained MAE [25], BEiT [1], and Swin Transformer [41], we also include the most recent SAR-specific approaches, including SAR-JEPA [32], SARATR-X [35], MSFA [38], and SUMMIT [16].

The scene classification and object detection comparison results are obtained from SAR-JEPA [32], SARATR-X [35], and SUMMIT [16], while the semantic segmentation results are directly sourced from AIR-PoSAR-Seg [95]. The downstream performance of ViT-B and ViT-L after pretraining is presented in the corresponding tables.

Target Classification. We first evaluate SARMAE on the target classification task, which does not require an additional decoder and therefore provides a direct assessment of the model’s representation capability. In implementation, the feature map from the last ViT layer is processed by global average pooling and then passed through a linear classifier to produce logits corresponding to the number of classes. We conduct experiments on three widely used datasets: FUSAR-SHIP [27], MSTAR [12],

and SAR-ACD [91]. We compare the performance of SAR-MAE with Copernicus FM [73] and CROMA [18], which adopts DINO distillation and contrastive learning respectively. Table 2 shows superior performance of SARMAE on FUSAR and SAR-ACD. Then, following the protocols in [16, 32], we adopt the 40-shot and 30% label settings for the FUSAR-SHIP and MSTAR datasets. As shown in Table 2, SARMAE consistently achieves state-of-the-art performance across all evaluation settings. For example, under the 30% label setting on FUSAR-SHIP, our ViT-B model reaches 92.92% accuracy, outperforming the previous best by a large margin of 21.01%. These results clearly demonstrate the effectiveness of our approach.

Horizontal & Oriented Object Detection. We then evaluate the transferability of the learned representations on the object detection task. For horizontal object detection, we use the classical SSDD [88] dataset and the more challenging SARDet-100k [38]. For oriented bounding box detection, we adopt the recently proposed large-scale RSAR dataset [90]. Following the fine-tuning protocols of [35], we integrate our pretrained backbones into Faster R-CNN [54] and Oriented R-CNN [87] for horizontal and oriented detection, respectively. The results are detailed in Table 3.

In the horizontal object detection scenario represented by SARDet-100k, our model with a standard ViT-B backbone achieves 57.9 mAP, slightly outperforming SARATR-X (built on HiViT-B) which reports 57.3 mAP. This result is particularly noteworthy because HiViT [89], with its hierarchical and pyramidal design, is generally regarded as an improved variant of ViT and typically delivers stronger performance. Nevertheless, our ViT-based model still attains the best results, underscoring that the performance gain primarily arises from the superior representations learned by SARMAE, rather than architectural advantages.

In the oriented object detection task, SARMAE also secures top performance with 66.8% mAP, surpassing existing methods by a large margin. Notably, our model exhibits excellent scalability: upgrading the backbone from ViT-B to ViT-L further boosts performance by +5.4 mAP, thereby widening the gap over previous approaches.

Semantic Segmentation. Beyond image-level and object-level evaluation, we further assess the pretrained model on pixel-level tasks through semantic segmentation. For this purpose, we adopt the well-known AIR-PoSAR-Seg dataset [95], which includes two settings: multiclass segmentation and single-class water extraction. Our implementation follows the protocol in [95], using UperNet [78] as the segmentation framework. As shown in Table 4, SARMAE achieves clear and consistent advantages over existing methods. By incorporating optical cues through SARC during pretraining, SARMAE captures clearer semantic structures, such as boundaries and texture structures, yielding superior segmentation results, particularly for the more chal-

lenging multiclass setting.

Method	Multiple classes							Water
	Industrial Area	Natural Area	Land Use	Water	Housing	Other	mIoU	IoU
FCN [44]	37.78	71.58	1.24	72.76	67.69	39.05	48.35	85.95
ANN [99]	41.23	72.92	0.97	75.95	68.40	56.01	52.58	87.32
PSPNet [92]	33.99	72.31	0.93	76.51	68.07	57.07	51.48	87.13
DeepLab V3+ [6]	40.62	70.67	0.55	72.93	69.96	34.53	48.21	87.53
PSANet [93]	40.70	69.46	1.33	69.46	68.75	32.68	47.14	86.18
DANet [17]	39.56	72.00	1.00	74.95	67.79	56.28	39.56	89.29
SARMAE(ViT-B)	65.87	75.65	29.20	84.01	73.23	71.21	66.53	92.31
SARMAE(ViT-L)	65.84	78.04	29.47	87.12	75.22	69.34	67.51	93.06

Table 4. Performance comparison of semantic segmentation methods on multiple classes and water classes.

4.2. Ablation Study

In this section, we investigate the effectiveness of the SAR-1M dataset and conduct ablation studies on SARMAE. We use a ViT-B model pretrained on ImageNet [11] with MAE [25] as our baseline to clearly highlight the contribution of each component in our method. All our ablation models training on SAR-1M use the same settings, i.e., 300 epochs, ensuring a controlled and fair comparison. For efficient verification, all ablation comparisons are conducted using the ViT-B backbone, and the effectiveness of each variant is demonstrated through fine-tuning on different downstream tasks.

Efficacy of SAR-1M. As shown in Table 5, we evaluate the impact of in-domain pretraining by applying the standard MAE framework across different datasets and fine-tuning on various SAR downstream tasks. It can be seen that, models pretrained from scratch on SAR-1M consistently outperform those pretrained on ImageNet or MillionAID. For example, on the FUSAR-SHIP classification benchmark, in-domain pretraining on SAR-1M improves accuracy from 75.40% (ImageNet) to 82.22%, yielding a substantial +6.82% absolute gain. Similarly, we observe improvements of +0.2 mAP on detection and +4.08 mIoU on segmentation. These results demonstrate that the unique characteristics of SAR imagery introduce a significant distribution gap from both natural and optical remote-sensing images, making it difficult for models pretrained on those modalities to transfer effectively. This underscores the necessity of constructing a large-scale SAR-specific pretraining dataset. Therefore, SAR-1M is not merely a large collection of images, but a high-quality, domain-aligned resource that facilitates the development of powerful representation models tailored for SAR imagery.

Ablation on SARE. We further validate the effectiveness of the SARE module by integrating it into the SAR-1M-pretrained MAE. As shown in Table 5, injecting physically grounded speckle noise yields consistent and substantial gains across all downstream tasks: classification accuracy on FUSAR-SHIP improves by +4.58%, and segmentation mIoU on AIR-PolSARSeg increases by +0.79%. These results support our central hypothesis that compelling the

Model	Pretrain Dataset	SARE	SARC	FUSAR	SSDD	AIR-PolSAR-Seg
MAE (Baseline)	ImageNet-1K [11]			75.40	64.00	60.28
MAE	MillionAID [45]			80.16	63.60	62.29
DINOv3	LVD-1689M [56]			74.25	61.60	58.42
MAE*	SAR-1M (only SAR)			82.22	64.20	64.36
MAE* (Add noise)	SAR-1M (only SAR)	✓		86.80	64.40	65.15
SARMAE*	SAR-1M (SAR/OPT)	✓	✓	89.30	68.10	66.53

Table 5. Ablation of SARE and SARC on multiple SAR datasets. *: Initialized with ImageNet pretrained MAE.

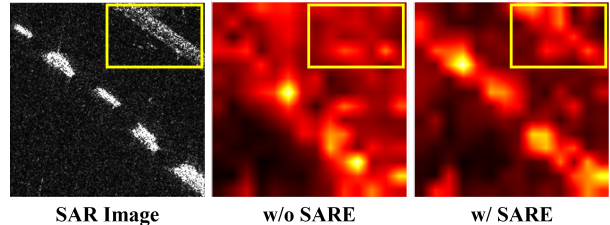


Figure 4. SARE significantly enhances the model’s semantic perception. Attention maps are computed by measuring the attention between the MAE encoder’s final-layer class token and image patch tokens.

model to reconstruct denoised targets enables it to better understand the noise characteristics of SAR imagery, thereby achieving noise-aware representation learning.

To provide more intuitive insights, we qualitatively examine how the model perceives scene content, as shown in Figure 4. With SARE, scene-relevant objects are more distinctly highlighted and exhibit clearer contours, indicating that the model can overcome noise interference and accurately capture semantic structures. Notably, the model is able to attend to subtle yet semantically relevant objects (see the yellow box), further indicating its enhanced ability to capture meaningful structures in noisy SAR imagery.

Ablation on SARC. Building upon MAE (add noise), we further evaluate the effectiveness of the SARC module by incorporating paired optical images during pretraining. As shown in Table 5, SARC yields consistent and significant improvements across all three downstream tasks. The effect is particularly notable on the SSDD detection benchmark, where performance increases by +3.7% (from 64.4% to 68.1%). In our experiments on this dataset, we observe that models often suffer from overfitting manifested as excessive false alarms, likely because the network misinterprets speckle noise as potential targets, indicating insufficient ability to capture true object semantics. By leveraging paired optical images, SARC provides clearer and more discriminative structural cues, enabling the model to better separate meaningful objects from noise. As a result, the detection accuracy improves substantially. Interestingly, although DINOv3 [56] has achieved remarkable performance on natural images, simply finetuning it on SAR images yields suboptimal results. This observation indicates that the effectiveness of SARC stems from explicit SAR-optical

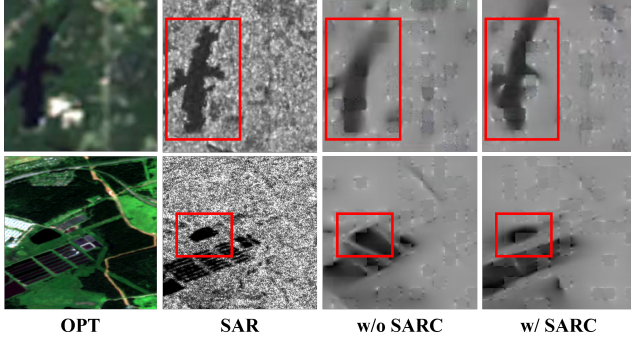


Figure 5. SARC leverages paired optical priors to recover the structural details of the original SAR image, which the model fails to reconstruct without this module.

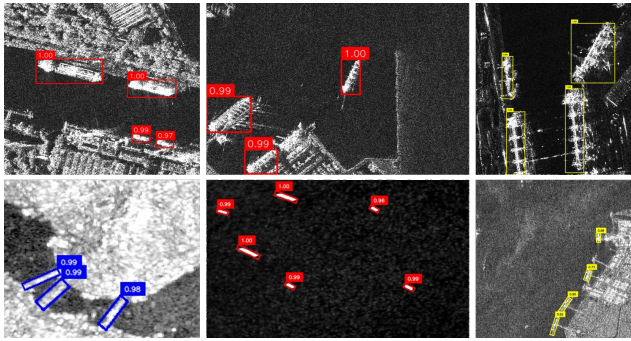


Figure 6. Visualization of Horizontal Object Detection Tasks on SSDD [88] and SAR-Det100k [38] in line 1. Oriented Object Detection Tasks on RSAR [90].

alignment, rather than from the strength of the optical backbone itself (i.e., DINOv3).

To further illustrate this mechanism, we visualize reconstructions from different pretrained MAE variants, as shown in Figure 5. With SARC, the model can recover the local scene structures present in the original SAR image (see the red box), whereas training on noisy SAR data alone results in blurred or incomplete reconstructions. This demonstrates that SARC injects clear optical semantic priors, enabling the model to discern true scene content and substantially enhancing the noise-aware masked image modeling process.

Based on the above ablation results, we find that SARE encourages the model to identify noise components irrelevant to scene understanding, enabling it to learn the correct information. In contrast, SARC introduces paired optical priors that guide the model toward clearer semantic structures. Together, these two components operate from complementary perspectives and jointly enhance the model’s representation and generalization ability on SAR imagery.

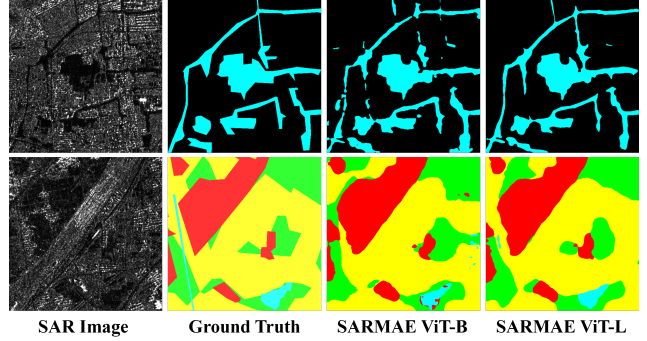


Figure 7. Visualization of segmentation tasks on AIR-PolSAR-Seg [95].

4.3. Visualization

Figure 6–7 present the qualitative results of our model on detection and segmentation tasks, respectively. As shown, our model can accurately detect targets of varying locations, shapes, and sizes in SAR imagery. In particular, for the challenging oriented detection scenario, our approach successfully captures the ship docked at the port with high confidence (see the yellow box in the second row of Figure 6), even though its appearance is difficult to distinguish from the surrounding environment. For single-class semantic segmentation, our model achieves robust performance: despite strong noise interference, it is still able to correctly identify water bodies with clear and coherent boundaries. In multi-class segmentation tasks, our method also produces segmentation maps of high visual quality. These results intuitively demonstrate the effectiveness of our approach.

5. Conclusion

In this paper, we present SARMAE, a self-supervised pre-training framework tailored for SAR representation learning. We introduce SAR-1M, the first million-scale SAR dataset with paired optical imagery, enabling large-scale pretraining directly aligned with SAR-specific characteristics. Building upon this, we propose two core innovations: Speckle-Aware Representation Enhancement (SARE), which explicitly models the statistical behavior of SAR speckle to learn noise-aware representations, and Semantic Anchor Representation Constraint (SARC), which leverages paired optical priors to guide SAR feature learning and improve semantic fidelity. Extensive experiments across classification, detection, and segmentation demonstrate that SARMAE achieves SOTA performance, validating both the quality of SAR-1M and the effectiveness of our pre-training framework. We believe that SAR-1M and SARMAE will constitute a strong foundation for future research in SAR representation learning and foster the development of SAR-oriented foundation models.

Acknowledgement

This work was supported in part by the Fundamental and Interdisciplinary Disciplines Breakthrough Plan of the Ministry of Education of China (JYB2025XDXM101), the National Natural Science Foundation of China (624B2109, 623B2079, 62225113), the Zhongguancun Academy Project (20240308), and the Key Technology Research Project of China National Petroleum Corporation (2025ZG82).

References

- [1] Hangbo Bao, Li Dong, Songhao Piao, and Furu Wei. Beit: Bert pre-training of image transformers. In *International Conference on Learning Representations*, 2022. 1, 6
- [2] Yee Kit Chan and Voon Koo. An introduction to synthetic aperture radar (sar). *Progress In Electromagnetics Research B*, 2:27–60, 2008. 1
- [3] Hongruixuan Chen, Jian Song, Olivier Dietrich, Clifford Broni-Bediako, Weihao Xuan, Junjue Wang, Xinlei Shao, Yimin Wei, Junshi Xia, Cuiling Lan, et al. Bright: A globally distributed multimodal building damage assessment dataset with very-high-resolution for all-weather disaster response. *Earth System Science Data Discussions*, 2025:1–51, 2025. 2
- [4] Haoyang Chen, Jing Zhang, Hebaixu Wang, Shiqin Wang, Pohsun Huang, Jiayuan Li, Haonan Guo, Di Wang, Zheng Wang, and Bo Du. Any2any: Unified arbitrary modality translation for remote sensing. *arXiv preprint arXiv:2603.04114*, 2026. 1
- [5] Jie Chen, Zhixiang Huang, Runfan Xia, Bocai Wu, Lei Sheng, Long Sun, and Baidong Yao. Large-scale multi-class sar image target detection dataset-1.0. *Journal of Radars*, 14: 1488, 2022. 2
- [6] Liang-Chieh Chen, Yukun Zhu, George Papandreou, Florian Schroff, and Hartwig Adam. Encoder-decoder with atrous separable convolution for semantic image segmentation. In *ECCV*, pages 801–818, 2018. 7
- [7] Ting Chen, Simon Kornblith, Mohammad Norouzi, and Geoffrey Hinton. A simple framework for contrastive learning of visual representations. In *ICML*, pages 1597–1607, 2020. 1
- [8] Xinlei Chen, Saining Xie, and Kaiming He. An empirical study of training self-supervised vision transformers. *CoRR*, abs/2104.02057, 2021. 2
- [9] Yezhen Cong, Samar Khanna, Chenlin Meng, Patrick Liu, Erik Rozi, Yutong He, Marshall Burke, David Lobell, and Stefano Ermon. Satmae: Pre-training transformers for temporal and multi-spectral satellite imagery. *NeurIPS*, 35:197–211, 2022. 2
- [10] Zhen Dai, Guangwen Mu, Wei Zha, and Renzheng Xu. A review on SAR image denoising algorithm using deep learning theory. In *Proceedings of the International Conference on Digital Image Processing*, page 1327419. International Society for Optics and Photonics, SPIE, 2024. 2
- [11] Jia Deng, Wei Dong, Richard Socher, Li-Jia Li, Kai Li, and Li Fei-Fei. Imagenet: A large-scale hierarchical image database. In *CVPR*, pages 248–255, 2009. 2, 5, 6, 7
- [12] Joseph R Diemunsch and John Wissinger. Moving and stationary target acquisition and recognition (mstar) model-based automatic target recognition: Search technology for a robust atr. In *Algorithms for Synthetic Aperture Radar Imaging V*, pages 481–492. SPIE, 1998. 2, 6, 3
- [13] Jian Ding, Nan Xue, Yang Long, Gui-Song Xia, and Qikai Lu. Learning roi transformer for detecting oriented objects in aerial images. *arXiv preprint arXiv:1812.00155*, 2018. 6
- [14] Dixon Domfeh and Saeid Safarveisi. Catnet: A geometric deep learning approach for cat bond spread prediction in the primary market. *arXiv preprint arXiv:2508.10208*, 2025. 6
- [15] Yuntao Du, Yushi Chen, Lingbo Huang, Yahu Yang, Pedram Ghamisi, and Qian Du. Summit: A sar foundation model with multiple auxiliary tasks enhanced intrinsic characteristics. *International Journal of Applied Earth Observation and Geoinformation*, 141:104624, 2025. 1, 2
- [16] Yuntao Du, Yushi Chen, Lingbo Huang, Yahu Yang, Pedram Ghamisi, and Qian Du. Summit: A sar foundation model with multiple auxiliary tasks enhanced intrinsic characteristics. *International Journal of Applied Earth Observation and Geoinformation*, 141:104624, 2025. 1, 2, 3, 6
- [17] Jun Fu, Jing Liu, Haijie Tian, Yong Li, Yongjun Bao, Zhiwei Fang, and Hanqing Lu. Dual attention network for scene segmentation. In *CVPR*, pages 3146–3154, 2019. 7
- [18] Anthony Fuller, Koreen Millard, and James Green. Croma: Remote sensing representations with contrastive radar-optical masked autoencoders. *NeurIPS*, 36:5506–5538, 2023. 2, 6
- [19] Anthony Fuller, Koreen Millard, and James Green. Croma: Remote sensing representations with contrastive radar-optical masked autoencoders. *NeurIPS*, 36:5506–5538, 2023. 2
- [20] Rudiger Gens and John L Van Genderen. Review article sar interferometry—issues, techniques, applications. *International Journal of Remote Sensing*, 17(10):1803–1835, 1996. 1
- [21] Ziyang Gong, Zhixiang Wei, Di Wang, Xiaoxing Hu, Xi-anzheng Ma, Hongruixuan Chen, Yuru Jia, Yupeng Deng, Zhenming Ji, Xiangwei Zhu, Xue Yang, Naoto Yokoya, Jing Zhang, Bo Du, Junchi Yan, and Liangpei Zhang. Crossearth: Geospatial vision foundation model for domain generalizable remote sensing semantic segmentation. *IEEE Transactions on Pattern Analysis and Machine Intelligence*, pages 1–18, 2025. 2
- [22] Jiaming Han, Jian Ding, Nan Xue, and Gui-Song Xia. Redet: A rotation-equivariant detector for aerial object detection. In *CVPR*, pages 2786–2795, 2021. 6
- [23] Kaiming He, Xiangyu Zhang, Shaoqing Ren, and Jian Sun. Deep residual learning for image recognition. In *CVPR*, pages 770–778, 2016. 6
- [24] Kaiming He, Haoqi Fan, Yuxin Wu, Saining Xie, and Ross Girshick. Momentum contrast for unsupervised visual representation learning. In *CVPR*, pages 9729–9738, 2020. 2
- [25] Kaiming He, Xinlei Chen, Saining Xie, Yanghao Li, Piotr Dollár, and Ross Girshick. Masked autoencoders are scalable vision learners. In *CVPR*, pages 16000–16009, 2022. 1, 2, 4, 5, 6, 7

- [26] Danfeng Hong, Bing Zhang, Xuyang Li, Yuxuan Li, Chenyu Li, Jing Yao, Naoto Yokoya, Hao Li, Pedram Ghamisi, Xiuping Jia, et al. Spectralgpt: Spectral remote sensing foundation model. *IEEE Transactions on Pattern Analysis and Machine Intelligence*, 2024. [2](#)
- [27] Xiyue Hou, Wei Ao, Qian Song, Jian Lai, Haipeng Wang, and Feng Xu. Fusar-ship: Building a high-resolution sar-ais matchup dataset of gaofen-3 for ship detection and recognition. *Science China Information Sciences*, 63(4):140303, 2020. [6](#), [2](#), [3](#), [4](#)
- [28] Gerhard Krieger. Mimo-sar: Opportunities and pitfalls. *IEEE Transactions on Geoscience and Remote Sensing*, 52(5):2628–2645, 2013. [1](#), [2](#)
- [29] Alex Krizhevsky, Ilya Sutskever, and Geoffrey E Hinton. Imagenet classification with deep convolutional neural networks. In *NeurIPS*. Curran Associates, Inc., 2012. [2](#)
- [30] Boying Li, Bin Liu, Lanqing Huang, Weiwei Guo, Zenghui Zhang, and Wenxian Yu. Opensarship 2.0: A large-volume dataset for deeper interpretation of ship targets in sentinel-1 imagery. In *SAR in Big Data Era: Models, Methods and Applications*, pages 1–5. IEEE, 2017. [2](#)
- [31] Feng Li, Shuya Chen, and Xin Zhang. Era-net: End-to-end recognition-aware sparse sar imaging network. In *IEEE International Conference on Signal, Information and Data Processing*, pages 1–5, 2024. [1](#)
- [32] Weijie Li, Wei Yang, Tianpeng Liu, Yuenan Hou, Yuxuan Li, Zhen Liu, Yongxiang Liu, and Li Liu. Predicting gradient is better: Exploring self-supervised learning for sar atr with a joint-embedding predictive architecture. *ISPRS Journal of Photogrammetry and Remote Sensing*, 218:326–338, 2024. [2](#), [3](#), [6](#)
- [33] Weijie Li, Wei Yang, Tianpeng Liu, Yuenan Hou, Yuxuan Li, Zhen Liu, Yongxiang Liu, and Li Liu. Predicting gradient is better: Exploring self-supervised learning for sar atr with a joint-embedding predictive architecture. *ISPRS Journal of Photogrammetry and Remote Sensing*, 218:326–338, 2024. [1](#)
- [34] Weijie Li, Wei Yang, Yuenan Hou, Li Liu, Yongxiang Liu, and Xiang Li. Saratr-x: Toward building a foundation model for sar target recognition. *IEEE Transactions on Image Processing*, 34:869–884, 2025. [1](#)
- [35] Weijie Li, Wei Yang, Yuenan Hou, Li Liu, Yongxiang Liu, and Xiang Li. Saratr-x: Towards building a foundation model for sar target recognition. *IEEE Transactions on Image Processing*, 2025. [1](#), [2](#), [3](#), [6](#)
- [36] Xingyu Li, Zhe Qu, Shangqing Zhao, Bo Tang, Zhuo Lu, and Yao Liu. Lomar: A local defense against poisoning attack on federated learning. *IEEE Transactions on Dependable and Secure Computing*, 20(1):437–450, 2021. [6](#)
- [37] Yanghao Li, Haoqi Fan, Ronghang Hu, Christoph Feichtenhofer, and Kaiming He. Scaling language-image pre-training via masking. In *CVPR*, pages 23390–23400, 2023. [2](#)
- [38] Yuxuan Li, Xiang Li, Weijie Li, Qibin Hou, Li Liu, Ming-Ming Cheng, and Jian Yang. Sardet-100k: Towards open-source benchmark and toolkit for large-scale sar object detection. *NeurIPS*, 37:128430–128461, 2024. [2](#), [3](#), [6](#), [8](#)
- [39] Tsung-Yi Lin, Priya Goyal, Ross Girshick, Kaiming He, and Piotr Dollár. Focal loss for dense object detection. In *ICCV*, pages 2980–2988, 2017. [6](#)
- [40] Xin Lin, Bo Zhang, Fan Wu, Chao Wang, Yali Yang, and Huiqin Chen. Sived: A sar image dataset for vehicle detection based on rotatable bounding box. *Remote Sensing*, 15(11), 2023. [2](#)
- [41] Ze Liu, Yutong Lin, Yue Cao, Han Hu, Yixuan Wei, Zheng Zhang, Stephen Lin, and Baining Guo. Swin transformer: Hierarchical vision transformer using shifted windows. In *ICCV*, pages 10012–10022, 2021. [6](#)
- [42] Zhuang Liu, Hanzi Mao, Chao-Yuan Wu, Christoph Feichtenhofer, Trevor Darrell, and Saining Xie. A convnet for the 2020s. In *CVPR*, pages 11976–11986, 2022. [6](#)
- [43] Ziyuan Liu, Shaoping Wang, and Yuantao Gu. Optimizing sar target detection through the multi-stage pre-training and fine-tuning strategy. In *Proceedings of the International Conference on Computer Science and Network Technology*, pages 178–181, 2024. [1](#)
- [44] Jonathan Long, Evan Shelhamer, and Trevor Darrell. Fully convolutional networks for semantic segmentation. In *CVPR*, pages 3431–3440, 2015. [7](#)
- [45] Yang Long, Gui-Song Xia, Shengyang Li, Wen Yang, Michael Ying Yang, Xiao Xiang Zhu, Liangpei Zhang, and Deren Li. Dirs: On creating benchmark datasets for remote sensing image interpretation. *arXiv preprint arXiv:2006.12485*, 2020. [7](#)
- [46] Jiming Lv, Daiyin Zhu, Zhe Geng, Shengliang Han, Yu Wang, Weixing Yang, Zheng Ye, and Tao Zhou. Recognition of deformation military targets in the complex scenes via minisar submeter images with fasar-net. *IEEE Transactions on Geoscience and Remote Sensing*, 61:1–19, 2023. [1](#)
- [47] Oscar Manas, Alexandre Lacoste, Xavier Giró-i Nieto, David Vazquez, and Pau Rodriguez. Seasonal contrast: Unsupervised pre-training from uncurated remote sensing data. In *ICCV*, pages 9414–9423, 2021. [2](#)
- [48] H McNairn and B Brisco. The application of c-band polarimetric sar for agriculture: A review. *Canadian Journal of Remote Sensing*, 30(3):525–542, 2004. [1](#)
- [49] Victor-Emil Neagoe, Serban-Vasile Carata, and Adrian-Dumitru Ciotec. An advanced neural network-based approach for military ground vehicle recognition in sar aerial imagery. *International Scientific Committee*, 41, 2016. [1](#)
- [50] Saurabh Parhad, Khushboo Warhade, and Sanjay Shitole. Speckle noise reduction in sar images using improved filtering and supervised classification. *Multimedia Tools and Applications*, 83:1–22, 2023. [2](#)
- [51] Xiaolei Qin, Di Wang, Jing Zhang, Fengxiang Wang, Xin Su, Bo Du, and Liangpei Zhang. Timo: Spatiotemporal foundation model for satellite image time series. *arXiv preprint arXiv:2505.08723*, 2025. [1](#)
- [52] Alec Radford, Jong Wook Kim, Chris Hallacy, Aditya Ramesh, Gabriel Goh, Sandhini Agarwal, Girish Sastry, Amanda Askell, Pamela Mishkin, Jack Clark, et al. Learning transferable visual models from natural language supervision. In *ICML*, pages 8748–8763. PmLR, 2021. [2](#)
- [53] Colorado J Reed, Ritwik Gupta, Shufan Li, Sarah Brockman, Christopher Funk, Brian Clipp, Kurt Keutzer, Salvatore

- Candido, Matt Uyttendaele, and Trevor Darrell. Scale-mae: A scale-aware masked autoencoder for multiscale geospatial representation learning. In *ICCV*, pages 4088–4099, 2023. 2
- [54] Shaoqing Ren, Kaiming He, Ross Girshick, and Jian Sun. Faster r-cnn: Towards real-time object detection with region proposal networks. *NeurIPS*, 28, 2015. 6, 4
- [55] Michael Schmitt, Lloyd Hughes, and Xiao Xiang Zhu. The sen1-2 dataset for deep learning in sar-optical data fusion. *ISPRS Annals of the Photogrammetry, Remote Sensing and Spatial Information Sciences*, pages 141–146, 2018. 3, 2
- [56] Oriane Siméoni, Huy V Vo, Maximilian Seitzer, Federico Baldassarre, Maxime Oquab, Cijo Jose, Vasil Khalidov, Marc Szafraniec, Seungeun Yi, Michaël Ramamonjisoa, et al. Dinov3. *arXiv preprint arXiv:2508.10104*, 2025. 4, 7, 3
- [57] Mannat Singh, Quentin Duval, Kalyan Vasudev Alwala, Haoqi Fan, Vaibhav Aggarwal, Aaron B. Adcock, Armand Joulin, Piotr Dollár, Christoph Feichtenhofer, Ross B. Girshick, Rohit Girdhar, and Ishan Misra. The effectiveness of mae pre-pretraining for billion-scale pretraining. *ICCV*, pages 5461–5471, 2023. 2
- [58] Xian Sun, Peijin Wang, Wanxuan Lu, Zicong Zhu, Xiaonan Lu, Qibin He, Junxi Li, Xuee Rong, Zhujun Yang, Hao Chang, et al. Ringmo: A remote sensing foundation model with masked image modeling. *IEEE Transactions on Geoscience and Remote Sensing*, 61:1–22, 2022. 2
- [59] Kiyo Tomiyasu. Tutorial review of synthetic-aperture radar (sar) with applications to imaging of the ocean surface. *Proceedings of the IEEE*, 66(5):563–583, 2005. 1
- [60] Arsenios Tsokas, Maciej Rysz, Panos M. Pardalos, and Kathleen Dipple. Sar data applications in earth observation: An overview. *Expert Systems with Applications*, 205: 117342, 2022. 1
- [61] Chao Wang, Wei Lu, Xiang Li, Jian Yang, and Lei Luo. M4-sar: A multi-resolution, multi-polarization, multi-scene, multi-source dataset and benchmark for optical-sar fusion object detection. *arXiv preprint arXiv:2505.10931*, 2025. 2
- [62] Di Wang, Qiming Zhang, Yufei Xu, Jing Zhang, Bo Du, Dacheng Tao, and Liangpei Zhang. Advancing plain vision transformer toward remote sensing foundation model. *IEEE Transactions on Geoscience and Remote Sensing*, 61:1–15, 2022. 2
- [63] Di Wang, Jing Zhang, Bo Du, Mingqiang Xu, Lin Liu, Dacheng Tao, and Liangpei Zhang. Samrs: Scaling-up remote sensing segmentation dataset with segment anything model. In *NeurIPS*, pages 8815–8827, 2023.
- [64] Di Wang, Jing Zhang, Mingqiang Xu, Lin Liu, Dongsheng Wang, Erzhang Gao, Chengxi Han, Haonan Guo, Bo Du, Dacheng Tao, and Liangpei Zhang. Mtp: Advancing remote sensing foundation model via multitask pretraining. *IEEE Journal of Selected Topics in Applied Earth Observations and Remote Sensing*, 17:11632–11654, 2024. 2
- [65] Di Wang, Meiqi Hu, Yao Jin, Yuchun Miao, Jiaqi Yang, Yichu Xu, Xiaolei Qin, Jiaqi Ma, Lingyu Sun, Chenxing Li, et al. Hypersigma: Hyperspectral intelligence comprehension foundation model. *IEEE Transactions on Pattern Analysis and Machine Intelligence*, 2025. 2
- [66] Fengxiang Wang, Hongzhen Wang, Di Wang, Zonghao Guo, Zhenyu Zhong, Long Lan, Wenjing Yang, and Jing Zhang. Harnessing massive satellite imagery with efficient masked image modeling. In *ICCV*, pages 6935–6947, 2025. 2
- [67] Fengxiang Wang, Yulin Wang, Mingshuo Chen, Haotian Wang, Hongzhen Wang, Haiyan Zhao, Yangang Sun, Shuo Wang, Di Wang, Long Lan, Wenjing Yang, and Jing Zhang. RoMA: Scaling up mamba-based foundation models for remote sensing. In *NeurIPS*, 2025. 2
- [68] Hebaixu Wang and Jiayi Ma. Deep adaptive unfolded network via spatial morphology stripping and spectral filtration for pan-sharpening. In *ICCV*, pages 10730–10740, 2025. 2
- [69] Hebaixu Wang, Jing Zhang, Haoyang Chen, Haonan Guo, Di Wang, Jiayi Ma, and Bo Du. Residual diffusion bridge model for image restoration. *arXiv preprint arXiv:2510.23116*, 2025.
- [70] Hebaixu Wang, Jing Zhang, Haonan Guo, Di Wang, Jiayi Ma, and Bo Du. Dgsolver: Diffusion generalist solver with universal posterior sampling for image restoration. *arXiv preprint arXiv:2504.21487*, 2025. 2
- [71] Hebaixu Wang, Jing Zhang, Haonan Guo, Di Wang, Jiayi Ma, Bo Du, and Liangpei Zhang. Universal pansharpening foundation model. *arXiv preprint arXiv:2603.03831*, 2026. 2
- [72] Yuanyuan Wang, Chao Wang, Hong Zhang, Yingbo Dong, and Sisi Wei. A sar dataset of ship detection for deep learning under complex backgrounds. *Remote Sensing*, 11(7):765, 2019. 2
- [73] Yi Wang, Zhitong Xiong, Chenying Liu, Adam J. Stewart, Thomas Dujardin, Nikolaos Ioannis Bountos, Angelos Zavras, Franziska Gerken, Ioannis Papoutsis, Laura Leal-Taixé, and Xiao Xiang Zhu. Towards a unified copernicus foundation model for earth vision. In *ICCV*, pages 9888–9899, 2025. 6
- [74] Zhirui Wang, Yuzhuo Kang, Xuan Zeng, et al. Sar-aircraft-1.0: High-resolution sar aircraft detection and recognition dataset. *Journal of Radars*, 12(4):906–922, 2023. 2
- [75] Shunjun Wei, Xiangfeng Zeng, Qizhe Qu, Mou Wang, Hao Su, and Jun Shi. Hrsid: A high-resolution sar images dataset for ship detection and instance segmentation. *Ieee Access*, 8: 120234–120254, 2020. 2
- [76] Gui-Song Xia, Xiang Bai, Jian Ding, Zhen Zhu, Serge J. Belongie, Jiebo Luo, Mihai Datcu, Marcello Pelillo, and Liangpei Zhang. Dota: A large-scale dataset for object detection in aerial images. *CVPR*, pages 3974–3983, 2017. 3
- [77] Junshi Xia, Hongruixuan Chen, Clifford Broni-Bediako, Yimin Wei, Jian Song, and Naoto Yokoya. Openearthmap-sar: A benchmark synthetic aperture radar dataset for global high-resolution land cover mapping. *arXiv preprint arXiv:2501.10891*, 2025. 2
- [78] Tete Xiao, Yingcheng Liu, Bolei Zhou, Yuning Jiang, and Jian Sun. Unified perceptual parsing for scene understanding. In *ECCV*, pages 418–434, 2018. 6
- [79] Zhitong Xiong, Yi Wang, Fahong Zhang, Adam J Stewart, Joëlle Hanna, Damian Borth, Ioannis Papoutsis, Bertrand Le Saux, Gustau Camps-Valls, and Xiao Xiang Zhu. Neural plasticity-inspired foundation model for observing the earth

- crossing modalities. *arXiv preprint arXiv:2403.15356*, 2024. **2**
- [80] Yoshio Yamaguchi. Disaster monitoring by fully polarimetric sar data acquired with alos-palsar. *Proceedings of the IEEE*, 100(10):2851–2860, 2012. **1**
- [81] Haodong Yang, Xinyue Kang, Long Liu, Yujiang Liu, and Zhongling Huang. Sar-hub: Pre-training, fine-tuning, and explaining. *Remote Sensing*, 15(23), 2023. **1**
- [82] Xue Yang, Junchi Yan, Ziming Feng, and Tao He. R3det: Refined single-stage detector with feature refinement for rotating object. In *AAAI*, pages 3163–3171, 2021. **6**
- [83] SHAO Yun, Tuya Hasi, et al. Research advances of sar remote sensing for agriculture applications: A review. *Journal of Integrative Agriculture*, 18(3):506–525, 2019. **1**
- [84] Ying Zeng, Xue Yang, Qingyun Li, Yushi Chen, and Junchi Yan. Ars-detr: Aspect ratio-sensitive detection transformer for aerial oriented object detection. *IEEE Transactions on Geoscience and Remote Sensing*, 62:1–15, 2023. **6**
- [85] Yikui Zhai, Wenlve Zhou, Bing Sun, Jingwen Li, Qirui Ke, Zilu Ying, Junying Gan, Chaoyun Mai, Ruggero Donida Labati, Vincenzo Piuri, et al. Weakly contrastive learning via batch instance discrimination and feature clustering for small sample sar atr. *IEEE Transactions on Geoscience and Remote Sensing*, 60:1–17, 2021. **2**
- [86] Peng Zhang, Hao Xu, Tian Tian, Peng Gao, Linfeng Li, Tianming Zhao, Nan Zhang, and Jinwen Tian. Sefepnet: Scale expansion and feature enhancement pyramid network for sar aircraft detection with small sample dataset. *IEEE Journal of Selected Topics in Applied Earth Observations and Remote Sensing*, 15:3365–3375, 2022. **2**
- [87] Shifeng Zhang, Longyin Wen, Xiao Bian, Zhen Lei, and Stan Z Li. Occlusion-aware r-cnn: Detecting pedestrians in a crowd. In *ECCV*, pages 637–653, 2018. **6**
- [88] Tianwen Zhang, Xiaoling Zhang, Jianwei Li, Xiaowo Xu, Baoyou Wang, Xu Zhan, Yanqin Xu, Xiao Ke, Tianjiao Zeng, Hao Su, et al. Sar ship detection dataset (ssdd): Official release and comprehensive data analysis. *Remote Sensing*, 13(18):3690, 2021. **2, 6, 8, 4**
- [89] Xiaosong Zhang, Yunjie Tian, Wei Huang, Qixiang Ye, Qi Dai, Lingxi Xie, and Qi Tian. Hivit: Hierarchical vision transformer meets masked image modeling. *arXiv preprint arXiv:2205.14949*, 2022. **3, 6**
- [90] Xin Zhang, Xue Yang, Yuxuan Li, Jian Yang, Ming-Ming Cheng, and Xiang Li. Rsar: Restricted state angle resolver and rotated sar benchmark. *CVPR*, 2025. **6, 8, 2**
- [91] Chenxi Zhao, Daochang Wang, Siqian Zhang, and Gangyao Kuang. Global discriminative information search and focus for sar target recognition. *IEEE Sensors Journal*, 25(9): 15735–15749, 2025. **6, 3, 4**
- [92] Hengshuang Zhao, Jianping Shi, Xiaojuan Qi, Xiaogang Wang, and Jiaya Jia. Pyramid scene parsing network. In *CVPR*, pages 2881–2890, 2017. **7**
- [93] Hengshuang Zhao, Yi Zhang, Shu Liu, Jianping Shi, Chen Change Loy, Dahua Lin, and Jiaya Jia. Psanet: Pointwise spatial attention network for scene parsing. In *ECCV*, 2018. **7**
- [94] Zhicheng Zhao, Changfu Zhou, Yu Zhang, Chenglong Li, Xiaoliang Ma, and Jin Tang. Text-guided coarse-to-fine fusion network for robust remote sensing visual question answering. *ISPRS Journal of Photogrammetry and Remote Sensing*, 230:1–17, 2025. **2**
- [95] WANG Zhirui, ZHAO Liangjin, WANG Yuelei, ZENG Xuan, KANG Jian, YANG Jian, and SUN Xian. Air-polsar-seg-2.0: Polarimetric sar ground terrain classification dataset for large-scale complex scenes. *Journal of Radars*, 14(2): 353–365, 2025. **6, 8, 2, 4**
- [96] Xiaoxiang Zhu, Sina Montazeri, Mohsin Ali, Yuansheng Hua, Yuanyuan Wang, Lichao Mou, Yilei Shi, Feng Xu, and Richard Bamler. Deep learning meets sar: Concepts, models, pitfalls, and perspectives. *IEEE Geoscience and Remote Sensing Magazine*, 9:143–172, 2020. **1**
- [97] Xizhou Zhu, Weijie Su, Lewei Lu, Bin Li, Xiaogang Wang, and Jifeng Dai. Deformable detr: Deformable transformers for end-to-end object detection. In *International Conference on Learning Representations*, 2020. **6**
- [98] Xiao Xiang Zhu, Sina Montazeri, Mohsin Ali, Yuansheng Hua, Yuanyuan Wang, Lichao Mou, Yilei Shi, Feng Xu, and Richard Bamler. Deep learning meets sar: Concepts, models, pitfalls, and perspectives. *IEEE Geoscience and Remote Sensing Magazine*, 9(4):143–172, 2021. **1**
- [99] Zhen Zhu, Mengde Xu, Song Bai, Tengting Huang, and Xi-ang Bai. Asymmetric non-local neural networks for semantic segmentation. In *ICCV*, pages 593–602, 2019. **7**

SARMAE: Masked Autoencoder for SAR Representation Learning

Supplementary Material

6. Overview

This supplementary material provides comprehensive details for the proposed SARMAE framework and the constructed SAR-1M dataset. These details were omitted from the main paper due to space constraints. The supplementary material is organized as follows:

- Section 7. Detailed composition and statistics of SAR-1M dataset;
- Section 8. Implementation details of Speckle-Aware Representation Enhancement (SARE);
- Section 12. Fine-tuning configurations for downstream tasks;
- Section 13. Extended visualization results;
- Section 14. Datasheet for SAR-1M.

7. Details for SAR-1M.

SAR-1M aggregates 18 publicly available SAR datasets, encompassing diverse imaging conditions, geographic locations, and task scenarios. Images in RSAR are the same in SAR-Det100k. Tab. 6 presents the detailed breakdown of each source dataset, including the image quantity, task type, image size, target type and spatial resolution. Datasets with paired SAR&OPT images are indicated in the last column, comprising 1,042,156 pairs in total.

SAR-1M encompasses 57 distinct categories, covering a diverse range of scene types. These categories span maritime objects, aerial targets, ground vehicles, infrastructure elements, land cover types, and event-related scenes, with visualizations of different scenarios, either SAR images or SAR-optical paired images, shown in Fig. 8-9.

SAR-1M employs hash-based deduplication to eliminate any potential overlap with the test sets of the downstream datasets used in the main paper. Even when trained on only 30% of SAR-1M (Tab. 7), SARMAE-S still outperforms SUMMIT, demonstrating both the stronger capacity of our model and the benefits brought by increased data scale.

8. Implementation Details of SARE

To enable the model to learn noise-aware representations while preserving its ability to reconstruct clean SAR imagery, we implement SARE through a carefully designed noise injection strategy during pretraining. Unlike conventional denoising approaches that process all samples uniformly, we adopt a probabilistic augmentation scheme in which each training iteration carries a 50% chance of applying synthetic noise corruption to the input. This dynamic sampling mechanism allows the encoder to simultaneously

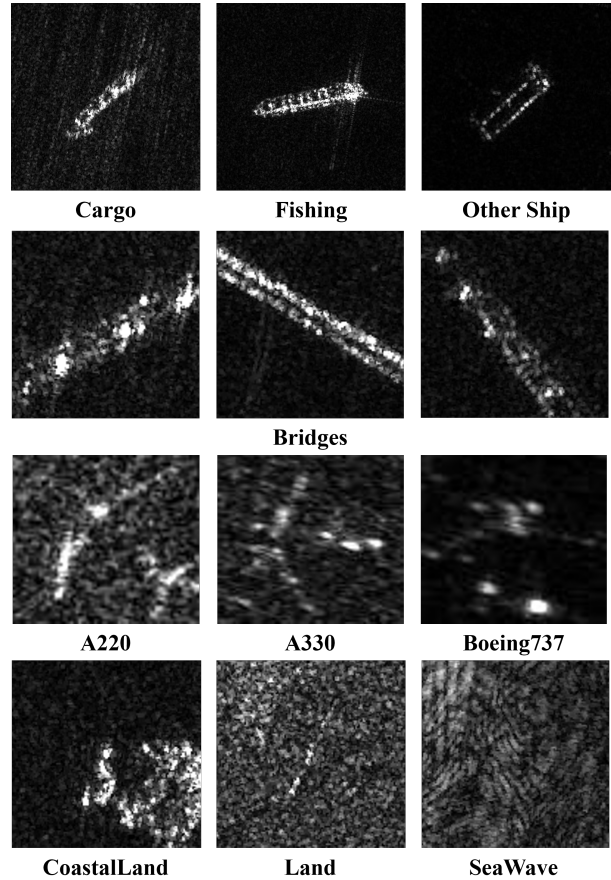


Figure 8. Various categories in SAR-1M.



Figure 9. Diverse scenes with SAR-OPT pairs in SAR-1M.

learn to reconstruct clean SAR content and to handle diverse noise characteristics.

Table 6. Detailed composition of SAR-1M dataset.

Dataset	Year	Tasks	Imgs.	Img. Size (px)	Targets (Cls.)	Res. (m)	Modality
MSTAR[12]	1995	Cls.	14,577	128~193	10	0.3	SAR
OpenSARShip[30]	2017	Cls.	26,679	9~445	14	2.3~17.4	SAR
SEN1-2[55]	2018	Det./Seg.	282,384	256	/	10	SAR&OPT
SAR-Ship[72]	2019	Det.	39,729	256	1	3~25	SAR
FUSAR-ship[27]	2020	Cls.	5,243	512	10	/	SAR
HRSID[75]	2020	Det./Seg.	89,664	256	1	0.5~3	SAR
SSDD[88]	2021	Det.	1,160	214~668	1	1~15	SAR
SADD[86]	2022	Det.	2,966	224	1	0.5~3	SAR
MSAR[5]	2022	Det.	28,499	256~2048	4	1	SAR
SAR-AIRcraft[74]	2023	Det.	18,818	512	7	1	SAR
SIVED[40]	2023	Det.	1,044	512	1	0.1~0.3	SAR
OGSOD[94]	2023	Det./Seg.	22,366	256	3	3	SAR
SAR-Det100k[38]	2024	Det.	94,493	512	6	0.5~25	SAR
RSAR[90]	2025	Det.	/	512	6	0.5~25	SAR
M4_SAR[61]	2025	Det.	448,696	256	6	10,60	SAR&OPT
Bright[3]	2025	Seg.	149,872	256	3	0.3~1	SAR&OPT
OpenEarthMap[77]	2025	Seg.	80,544	256	8	0.15~0.5	SAR&OPT
AIR-PoSAR-Seg[95]	2025	Det./Seg.	6,168	512	6	8	SAR
SAR-1M	2025	Cls./Det./Seg.	1,312,902	9~2048	57	0.1~60	SAR&OPT

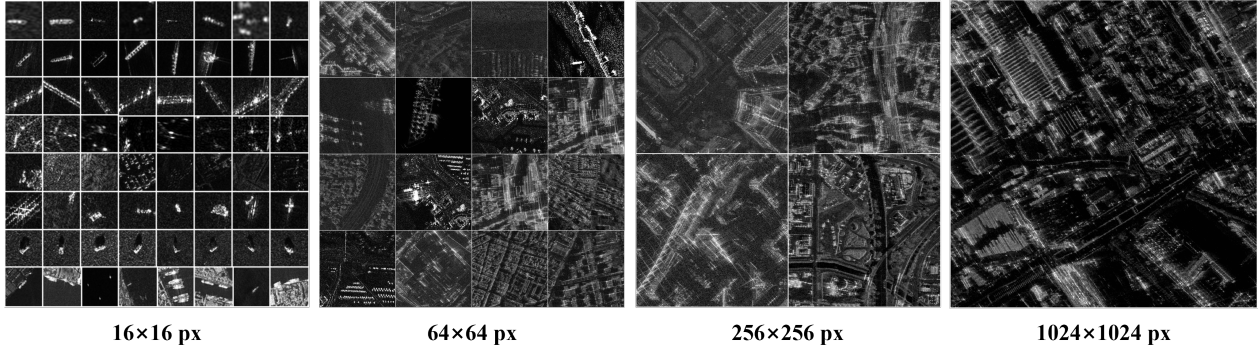


Figure 10. Images of different resolutions in SAR-1M.

When an image is selected for augmentation, one of four physically motivated noise models is randomly chosen and applied.

The first category is additive Gaussian noise, which simulates random interference and is defined as:

$$x'(i, j) = x(i, j) + \mathcal{N}(0, \sigma^2), \quad (9)$$

where σ is randomly sampled from the range $[0.0, 0.5]$ to represent different noise levels.

The second category introduces multiplicative Rayleigh noise, which models the amplitude statistics of single-look SAR data:

$$x'(i, j) = x(i, j) \cdot \mathcal{R}(\sigma), \quad (10)$$

where $\mathcal{R}(\sigma)$ denotes a Rayleigh-distributed random vari-

able with scale parameter σ sampled from $[0.0, 0.5]$.

The third noise type is Gamma-distributed multiplicative noise, representing the multi-look SAR intensity formation described in Eq.1 of the main text:

$$x'(i, j) \sim \text{Gamma}(L_{\text{syn}}, x(i, j)/L_{\text{syn}}), \quad (11)$$

where the synthetic look number L_{syn} is randomly selected from 1, 2, 3, 4 to yield varying noise intensity levels.

The fourth category is additive uniform noise, which simulates sensor-induced perturbations. It is formulated as:

$$x'(i, j) = x(i, j) + \mathcal{U}(-\alpha, \alpha), \quad (12)$$

where $\mathcal{U}(-\alpha, \alpha)$ denotes a uniform random variable drawn from the interval $[-\alpha, \alpha]$, and α is randomly sampled from $[0.0, 0.5]$ to control the perturbation magnitude.

Table 7. Comparison of performance across different datasets. All models adopt ViT-B as the backbone.

Model	Dataset	Dataset Scale	FUSAR_30% [27]	SAR-ACD [91]
SUMMIT [16]	MuSID	560k	71.91	84.25
SARMAE-S	SAR-1M(30%)	300k	88.27	93.76
SARMAE	SAR-1M	1000k	92.92	95.06

Each chosen noise model further samples its related hyperparameters from the corresponding ranges, ensuring diverse corruption patterns both across iterations and within each training batch.

During training, if augmentation is applied, the corrupted image x' is masked and encoded following the MAE protocol, while the reconstruction target remains the original clean patch x . This formulation compels the encoder to map noisy, incomplete inputs back to clean and complete scene content. For iterations where augmentation is skipped, standard MAE reconstruction is performed without synthetic noise. This probabilistic dual-mode training paradigm enables SARMAE to learn noise-robust and semantically rich representations without compromising reconstruction quality or training stability.

Pretraining with pseudo-clean targets generated by SAR denoisers (LEE, BM3D, FROST) yields suboptimal classification accuracy (Tab. 8), as such targets often distort semantic structures. SARE learns to adaptively model complex SAR noise and capture task-relevant representations. As shown in Tab. 9, SARE outperforms both standard MAE and Gaussian denoising baselines. These results provide strong evidence that physics-driven noise modeling in SARE offers more robust SAR representations than standard augmentation strategies.

Table 8. Classification accuracy by pretraining on varied denoiser.

Denoiser	None	LEE	BM3D	FROST
MSTAR [12]	90.66	77.81	82.16	76.30

9. Implementation Details of SARC

We exclude optical images with cloud cover $\geq 20\%$ to ensure data quality. To avoid over-regularization from the optical modality, SARC is assigned a low loss weight ($\lambda = 0.1$), and additional unpaired SAR samples (0.3M) are incorporated to preserve feature autonomy in the SAR branch. As shown in Tab. 9, replacing SARC with contrastive loss leads to performance degradation, likely because speckle noise in SAR imagery makes negative pairs highly unreliable and interferes with stable feature alignment. In contrast, cosine similarity focuses on aligning positive pairs without aggressive repulsion, which is more suitable for bridging these distinct modalities. Moreover, Tab. 9 shows

that SARE and SARC complement each other, yielding further performance gains when combined.

10. Rationale for DINOv3

DINOv3 [56] offers superior optical representations, compared to ImageNet pretrained MAE-ViT (see Tab. 10, both models adopt the Base version). We froze DINOv3 encoder to prevent it from adapting to SAR domain, which provides purely semantic guidance in the optical modality.

11. Model Scalability Analysis

In terms of efficiency, scaling from ViT-B to ViT-L introduces a moderate training overhead (+33%) on $8 \times A800$ GPUs (Tab. 11), indicating that SARMAE scales efficiently with model size. While ViT-L tends to overfit on smaller datasets (FUSAR-SHIP, MSTAR) due to its higher capacity, it consistently outperforms ViT-B on large-scale benchmarks (SARDet-100K). These results suggest that SARMAE follows standard scaling behavior, where larger models benefit from sufficient training data.

12. Fine-tuning Configurations for Downstream Tasks

All experiments are conducted using the pretrained ViT-B and ViT-L backbones initialized with SARMAE weights. And all experiments are conducted on 8 NVIDIA A800 GPUs (40GB). We use PyTorch Distributed Data Parallel (DDP) for multi-GPU training. Gradient clipping with a maximum norm of 1.0 is applied across all tasks. For ViT-L models, we apply checkpoints to maintain the effective batch size when GPU memory is limited.

12.1. Target Classification

For target classification tasks, we evaluate SARMAE on three datasets: FUSAR-SHIP [27], MSTAR [12], and SAR-ACD [91]. The pretrained ViT encoder is adapted for classification by appending a global average pooling layer followed by a linear classification head. The number of output dimension in the linear layer corresponds to the number of classes in each dataset. The training configurations are detailed in Tab. 12. For the 40-shot experiments on FUSAR-SHIP and MSTAR, we randomly sample 40 images per class for training while using the full test set for evaluation. For the 30% labeled setting on FUSAR-SHIP,

Table 9. Ablation study on noise addition and loss functions.

Model	Noise Addition	Loss Function	FUSAR.40 [27]	SSDD [88]	AIR-PolSAR-Seg [95]
MAE [25]	-	-	82.22	64.20	64.36
MAE + G	Gaussian	-	85.16	62.60	63.19
SARE	Ours	-	86.80	<u>64.40</u>	<u>65.15</u>
SARE + C	Ours	Contrastive Loss	<u>86.95</u>	62.40	63.41
SARMAE	Ours	SARC	89.30	68.10	66.53

Table 10. Comparison of different teachers for the Optical Branch. ViT-B is adopted as the backbone.

Optical Branch Init.	FUSAR.40 [27]	SAR-ACD [91]
MAE-ViT [25]	84.29	89.87
DINOv3 [56] (Ours)	89.30	95.06

Table 11. Efficiency Analysis.

Model	Params (M)	FLOPs (G)	Training Cost (h)
ViT-B (Baseline)	86	17.6	~45
ViT-L	307	61.6	~60

MSTAR and SAR-ACD, we randomly select 30% of the training data while keeping the test set unchanged. Each experiment is repeated 3 times with different random seeds, and we report the average accuracy.

12.2. Horizontal&Oriented Object Detection

For horizontal bounding box detection, we integrate the pre-trained SARMAE backbone into the Faster R-CNN [54] framework with a Feature Pyramid Network (FPN) neck. We evaluate on two datasets: SSDD and SARDet-100k. And for oriented bounding box detection on the RSAR dataset, we adopt Oriented R-CNN as the detection framework, which extends Faster R-CNN with rotated Region of Interest (RoI) features and oriented bounding box regression. The training configurations are detailed in Tab. 12. To preserve the pretrained representations, we freeze all layers of the ViT backbone except the final layer during fine-tuning. This approach maintains the general SAR features learned during pretraining while allowing task-specific adaptation through the detection head.

12.3. Semantic Segmentation

For pixel-level semantic segmentation on the AIR-PolSAR-Seg dataset, we utilize UperNet as the segmentation framework. For the multi-class segmentation task, we report mean Intersection over Union (mIoU) across all categories. For the single-class water extraction task, we report the IoU for the water class. The training settings have been shown in Tab. 12.

13. Extended visualization results

Fig. 11 presents detection results on SSDD, SARDet-100k, and RSAR datasets. The visualizations demonstrate the model’s capability to accurately localize ships in diverse scenarios, including multi-scale detection, dense harbor scenes, and oriented bounding box prediction for arbitrarily-oriented vessels.

Fig. 12 illustrates semantic segmentation results on AIR-PolSAR-Seg dataset. The model achieves precise pixel-level classification for multiple terrain categories and accurate water body extraction, demonstrating strong performance on fine-grained segmentation tasks.

14. Datasheets

14.1. Motivation

The questions in this section are primarily intended to encourage dataset creators to clearly articulate their reasons for creating the dataset and to promote transparency about funding interests. The latter may be particularly relevant for datasets created for research purposes.

1. “*For what purpose was the dataset created?*”

A: SAR-1M was created to address the lack of large-scale, diverse SAR datasets for self-supervised representation learning. Existing SAR datasets are limited in scale (100k-500k) and diversity, hindering the development of foundation models for SAR imagery.

2. “*Who created the dataset (e.g., which team, research group) and on behalf of which entity?*”

A: The dataset was curated by us as part of research on SAR representation learning. It aggregates 18 publicly available SAR datasets.

3. “*Who funded the creation of the dataset?*”

A: The dataset creation was funded by the affiliations of the authors involved in this work.

14.2. Composition

Most of the questions in this section are intended to provide dataset consumers with the information they need to make informed decisions about using the dataset for their chosen tasks. Some of the questions are designed to elicit information about compliance with the EU’s General Data Protec-

Table 12. Training configurations for different tasks.

Config	Classification	Detection	Segmentation
optimizer	AdamW	AdamW	AdamW
base learning rate	1.0×10^{-3}	1.0×10^{-4}	6.0×10^{-5}
weight decay	0.05	0.05	0.05
optimizer momentum	$\beta_1, \beta_2 = 0.9, 0.95$	$\beta_1, \beta_2 = 0.9, 0.95$	$\beta_1, \beta_2 = 0.9, 0.99$
batch size	25	16	4
learning rate schedule	Cosine	Step	Polynomial
warmup iterations	2000	1000	1500
warmup type	Constant	Linear	Linear
warmup learning rate	1.0×10^{-5}	0.33333	6.0×10^{-8}

tion Regulation (GDPR) or comparable regulations in other jurisdictions. Questions that apply only to datasets that relate to people are grouped together at the end of the section. We recommend taking a broad interpretation of whether a dataset relates to people. For example, any dataset containing text that was written by people relates to people.

1. “What do the instances that comprise our datasets represent (e.g., documents, photos, people, countries)?”
A: The dataset primarily comprises SAR imagery captured by satellites. All datasets utilized in SAR-IM are publicly accessible and nonprofif.
2. “How many instances are there in total (of each type, if appropriate)?”
A: SAR-IM contains 1.3 million SAR image instances captured by satellites and 1 million paired SAR-OPT, 2.3 million in total.
3. “Does the dataset contain all possible instances or is it a sample (not necessarily random) of instances from a larger set?”
A: Yes, our dataset contains all possible instances that have been collected so far.
4. “Is there a label or target associated with each instance?”
A: No, our dataset is intended for self-supervised learning. Therefore, each instance is an individual SAR/OPT image and does not contain annotations.
5. “Is any information missing from individual instances?”
A: No.
6. “Are relationships between individual instances made explicit (e.g., users’ movie ratings, social network links)?”
A: Yes, the relationship between individual instances is explicit.
7. “Are there recommended data splits (e.g., training, development/validation, testing)?”
A: Yes, the entire dataset is intended for self-supervised methods, and we recommend using the whole dataset for self-supervised learning research.
8. “Is the dataset self-contained, or does it link to or oth-

erwise rely on external resources (e.g., websites, tweets, other datasets)?”

- A:** Yes, our dataset relies on many publicly available SAR datasets, which we have detailed in the main text.
9. “Does the dataset contain data that might be considered confidential (e.g., data that is protected by legal privilege or by doctor–patient confidentiality, data that includes the content of individuals’ non-public communications)?”
A: No, all data are clearly licensed.
 10. “Does the dataset contain data that, if viewed directly, might be offensive, insulting, threatening, or might otherwise cause anxiety?”
A: No.

14.3. Collection Process

In addition to the goals outlined in the previous section, the questions in this section are designed to elicit information that may help researchers and practitioners create alternative datasets with similar characteristics. Again, questions that apply only to datasets that relate to people are grouped together at the end of the section.

1. “How was the data associated with each instance acquired?”
A: Please refer to the details listed in the main text Sec. 2.
2. “What mechanisms or procedures were used to collect the data (e.g., hardware apparatuses or sensors, manual human curation, software programs, software APIs)?”
A: Please refer to the details listed in the main text Sec. 2.
3. “If the dataset is a sample from a larger set, what was the sampling strategy (e.g., deterministic, probabilistic with specific sampling probabilities)?”
A: Please refer to the details listed in the main text Sec. 2.

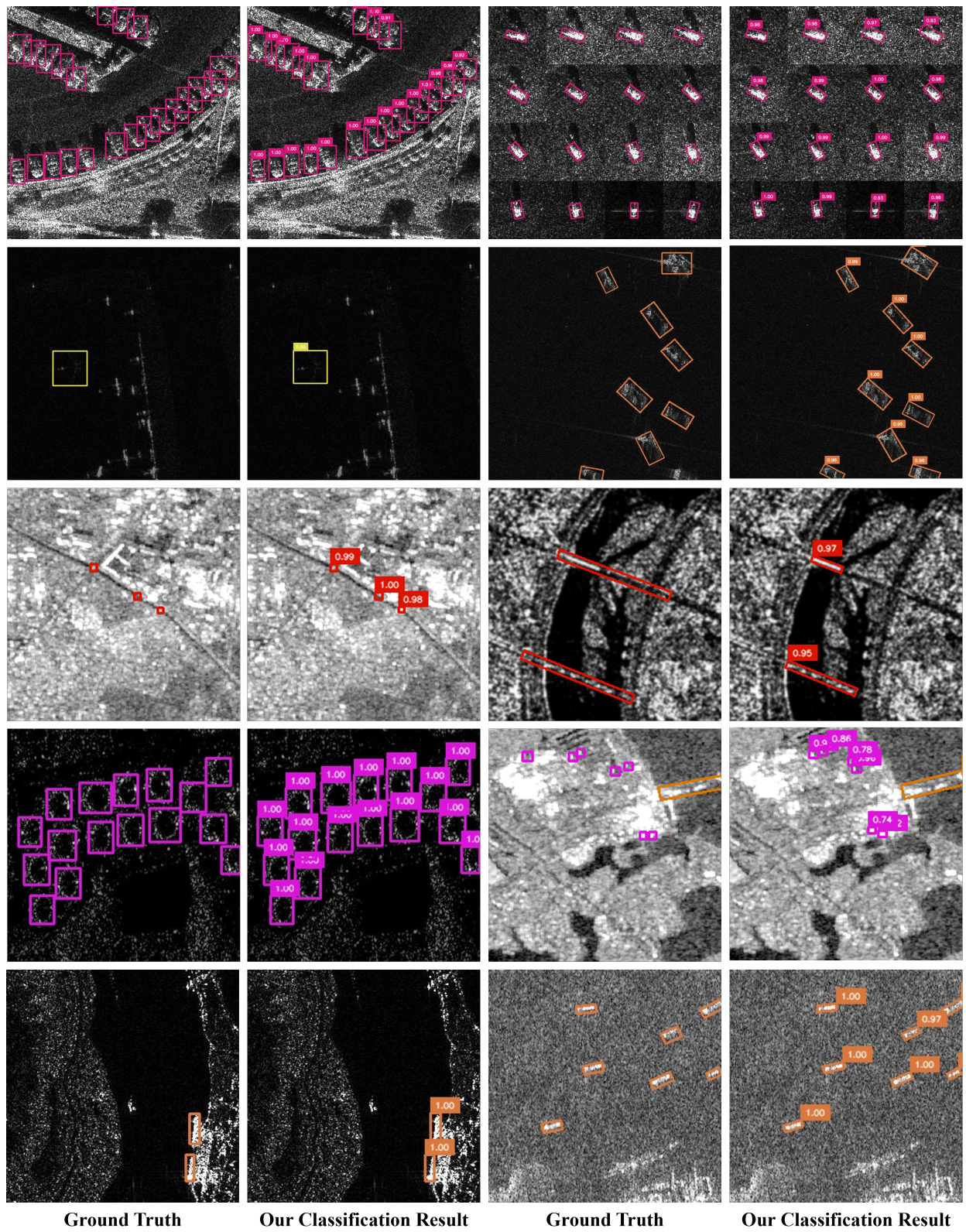


Figure 11. Object detection visualization results.

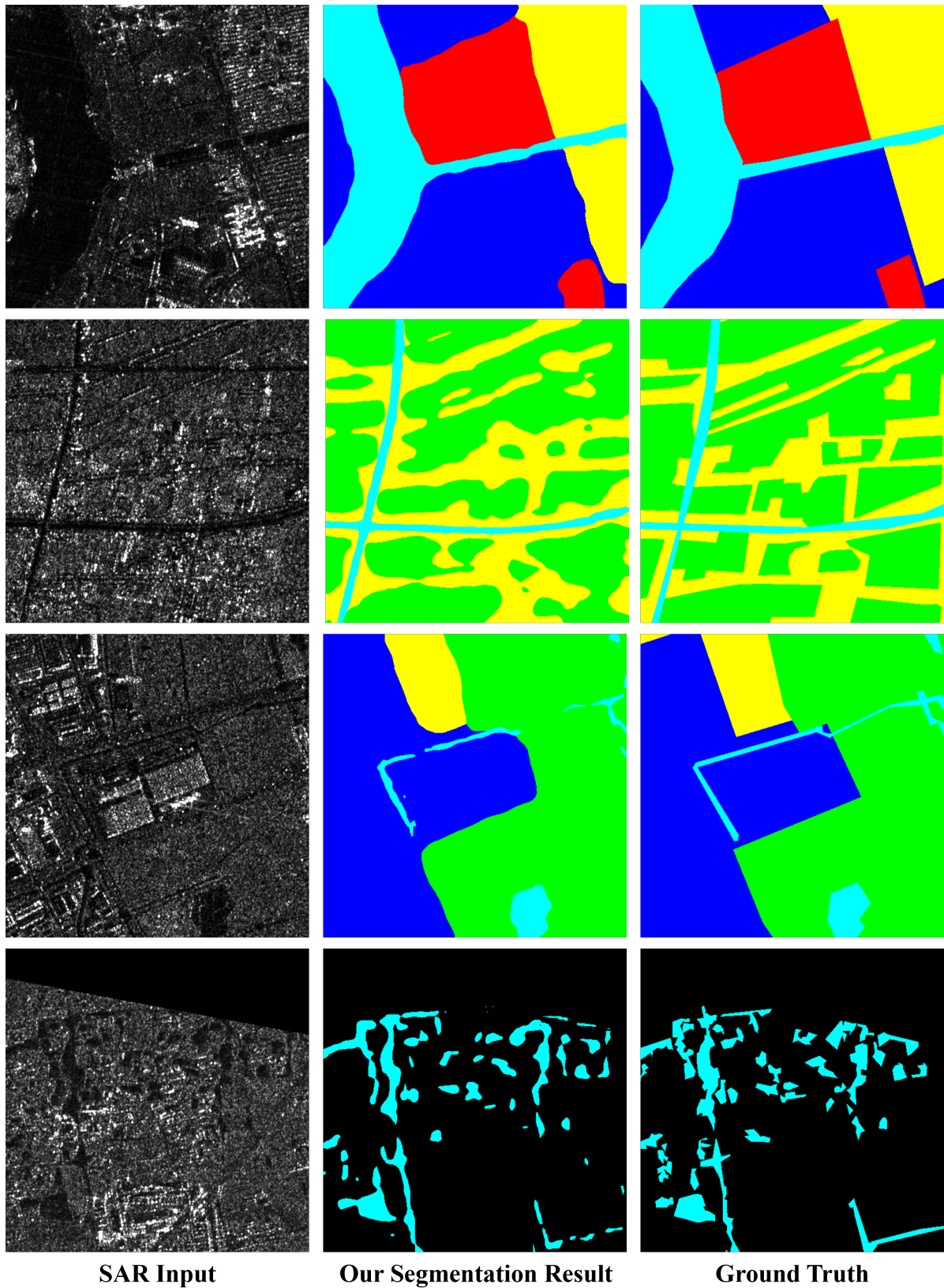


Figure 12. Semantic segmentation visualization results. Blue: Industrial. Green: Natural. Red: Land Use. Cyan: Water. White: Other. Yellow: Housing.

14.4. Preprocessing, Cleaning, and Labeling

The questions in this section are intended to provide dataset consumers with the information they need to determine whether the “raw” data has been processed in ways that are compatible with their chosen tasks. For example, text that has been converted into a “bag-of-words” is not suitable for tasks involving word order.

1. “Was any preprocessing/cleaning/labeling of the data done (e.g., discretization or bucketing, tokenization, part-of-speech tagging, SIFT feature extraction, removal of instances, processing of missing values)?”

A: Yes, we preprocessed and cleaned data in our dataset.

2. “Was the ‘raw’ data saved in addition to the preprocessed/cleaned/labeled data (e.g., to support unanticipated future uses)?”

A: Yes, raw data is accessible.

3. “Is the software that was used to preprocess/clean/label the data available?”

A: Yes, the necessary software used to preprocess and clean the data is publicly available.

14.5. Uses

The questions in this section are intended to encourage dataset creators to reflect on tasks for which the dataset should and should not be used. By explicitly highlighting these tasks, dataset creators can help dataset consumers make informed decisions, thereby avoiding potential risks or harms.

1. “Has the dataset been used for any tasks already?”

A: No.

2. “Is there a repository that links to any or all papers or systems that use the dataset?”

A: Not yet, but we will provide such links in our GitHub repository soon in the future.

3. “What (other) tasks could the dataset be used for?”

A: The dataset could be used for training the SAR foundation models with the self-supervised learning method.

4. “Is there anything about the composition of the dataset or the way it was collected and preprocessed/cleaned/labeled that might impact future uses?”

A: N/A.

5. “Are there tasks for which the dataset should not be used?”

A: N/A.

14.6. Distribution

Dataset creators should provide answers to these questions prior to distributing the dataset either internally within the entity on behalf of which the dataset was created or externally to third parties.

1. “Will the dataset be distributed to third parties outside of the entity (e.g., company, institution, organization) on behalf of which the dataset was created?”

A: No.

2. “How will the dataset be distributed (e.g., tarball on website, API, GitHub)?”

A: Very likely to be distributed by website, API, and GitHub repository.

3. “When will the dataset be distributed?”

A: The datasets are publicly accessible, our SAR-1M will be publicly available soon.

4. “Will the dataset be distributed under a copyright or other intellectual property (IP) license, and/or under applicable terms of use (ToU)?”

A: Yes, the dataset is under the Creative Commons Attribution-NonCommercial-ShareAlike 4.0 International License.

5. “Have any third parties imposed IP-based or other restrictions on the data associated with the instances?”

A: No.

6. “Do any export controls or other regulatory restrictions apply to the dataset or to individual instances?”

A: No.

14.7. Maintenance

As with the questions in the previous section, dataset creators should provide answers to these questions prior to distributing the dataset. The questions in this section are intended to encourage dataset creators to plan for dataset maintenance and communicate this plan to dataset consumers.

1. “Who will be supporting/hosting/maintaining the dataset?”

A: The authors of this work serve to support, host, and maintain the datasets.

2. “How can the owner/curator/manager of the dataset be contacted (e.g., email address)?”

A: The curators can be contacted via the email addresses listed on our webpage.

3. “Is there an erratum?”

A: There is no explicit erratum; updates and known errors will be specified in future versions.

4. “Will the dataset be updated (e.g., to correct labeling errors, add new instances, delete instances)?”

A: Yes, for the current version. Future updates (if any) will be posted on the dataset website.

5. “Will older versions of the dataset continue to be supported/hosted/maintained?”

A: Yes. This is the first version of the release; future updates will be posted and older versions will be replaced.

6. “If others want to extend/augment/build on/contribute to the dataset, is there a mechanism for them to do so?”

A: Yes, we provide detailed instructions for future extensions.